Size-Selected Graphene Oxide Loaded with Photosensitizer (TMPyP) for Targeting Photodynamic Therapy In Vitro

Kateřina Bartoň Tománková [1], Ariana Opletalová [2], Kateřina Poláková [2,*], Sergii Kalytchuk [2], Jana Jiravová [1], Jakub Malohlava [1], Lukáš Malina [1] and Hana Kolářová [1]

[1] Department of Medical Biophysics, Faculty of Medicine and Dentistry, Institute of Translational Medicine, Palacký University Olomouc, Hněvotínská 3, 775 15 Olomouc, Czech Republic; katerina.barton@upol.cz (K.B.T.); jana.jiravova@upol.cz (J.J.); malohlava.jakub@gmail.com (J.M.); lukas.malina@upol.cz (L.M.); hana.kolarova@upol.cz (H.K.)

[2] Regional Centre of Advanced Technologies and Materials, Faculty of Science, Palacký University, Šlechtitelů 27, 771 46 Olomouc, Czech Republic; ariana.opletalova@upol.cz (A.O.); sergii.kalytchuk@upol.cz (S.K.)

[*] Correspondence: katerina.polakova@upol.cz; Tel.: +420-5856-34473

check for updates

Abstract: Targeted therapies of various diseases are nowadays widely studied in many biomedical fields. Photodynamic therapy (PDT) represents a modern treatment of cancer using a locally activated light. TMPyP is an efficient synthetic water-soluble photosensitizer (PS), yet with poor absorption in the visible and the red regions. In this work, we prepared size-selected and colloidally stable graphene oxide (GO) that is appropriate for biomedical use. Thanks to the negative surface charge of GO, TMPyP was easily linked in order to create conjugates of GO/TMPyP by electrostatic force. Due to the strong ionic interactions, charge transfers between GO and TMPyP occur, as comprehensively investigated by steady-state and time-resolved fluorescence spectroscopy. Biocompatibility and an in vitro effect of GO/TMPyP were confirmed by a battery of in vitro tests including MTT, comet assay, reactive oxygen species (ROS) production, and monitoring the cellular uptake. PDT efficiency of GO/TMPyP was tested using 414 and 740 nm photoexcitation. Our newly prepared nanotherapeutics showed a higher PDT effect than in free TMPyP, and is promising for targeted therapy using clinically favorable conditions.

Keywords: size reduced graphene oxide; photosensitizer; TMPyP; in vitro; photodynamic therapy

1. Introduction

Cancer is still one of the death leading diseases and, according to the World Health Organization (WHO), accounts for ~15% of the total human deaths [1–3]. Conventional clinical treatments such as radiation therapy, surgery, and chemotherapy, alone or with combination, show limited efficacy along with systemic toxicity and harm to the surrounding healthy tissue [4]. Therefore, early diagnosis and effective treatments are still the most challenging tasks in today's medicine. Among various cancer treatment strategies, phototherapies have attracted attention due to minimal invasiveness, deeper tissue penetration, less damage to non-cancerous tissues, and resulting in reduced systemic toxicity [5].

In general, in photodynamic therapy (PDT), local, systemic, or topical injection of a nontoxic drug/dye known as photosensitizer (PS) is administered at the targeted site, followed by appropriate illumination from an external source. In fact, PS absorbs the selective wavelength of light, reaches the excited state, and, during the returning to the ground state, transfers its energy to the local oxygen molecules, which in turn leads to the production of reactive oxygen species (ROS) including mainly $^1O_2$.

This ROS can activate pro-apoptotic signals and consequently cause programmed cancer cell death leading to complete tumor destruction [4,6]. The efficiency of PS is strongly given by the wavelength of the activated light influencing the depth of the penetration into the tissue and final production of ROS [7].

There are four main classes of photosensitizers (first generation) such as porphyrin derivatives, chlorins, phthalocyanines, and porphycenes, which exhibit different mechanisms of action and light activation [8]. However, most organic PS molecules can be activated by visible or UV light only. Near-infrared radiation (NIR) activation of organic PS in PDT is very rare [4,9]. In order to improve the PDT effect, the second generation of photosensitizers has been developed. They are activated at longer wavelengths, which increases tissue penetration [10]. The third generation of photosensitizers is made of the second generation conjugated with various biomolecules or nanoparticles for better targeting and working in near-infrared radiation (NIR). It is highly desirable to develop an effective and biocompatible light-sensitive agent, which can operate under ultra-low-light doses.

TMPyP, the cationic 5,10,15,20-tetrakis(1-methyl4-pyridinio) porphyrin tetra(p-toluensulfonate) is a modern type of synthetic, water-soluble PS. However, TMPyP is still a porphyrin derivative of a second generation with the main absorption band around 420 nm and low absorption bands in the visible regions [11]. Due to the short wavelength, photons cannot penetrate deeply into the tissue.

However, over the past decades, nanotechnology has become a promising strategy leading to personalized medicine, where the synthesis of new nanomaterials plays a significant role in drug delivery systems. In fact, nanotechnology designs nanomaterials with multifunctional properties that can be used in diagnostics and therapeutics at the same time [12,13]. These nanocarriers or nanodrugs can be delivered directly to the target sites, preventing side effects in healthy tissues. Nowadays, clinical trials of various nanosystems for treatment and diagnostics are performed in order to achieve the most desirable outcomes [14].

Recently, graphene and graphene oxide (GO) have been considered some of the most promising nanomaterials for bioapplications. Unique properties, such as enormous large surface area due to the two-dimensional planar structure, chemical and mechanical inertness, high conductivity, and sufficient biocompatibility, make graphene derivatives very promising nanocarriers for advanced drug delivery and targeted delivery of various therapeutics [15–19]. For immobilization of drugs on the surface of GO, noncovalent methods including surface adsorption, hydrogen bonding, and other types of interactions can be easily used. Concerning the surface chemistry, pristine graphene is highly hydrophobic and poorly dispersible in water; however, GO is hydrophilic and dispersible in water, which makes GO a highly suitable PS-nanocarrier [20,21].

In this work, we verified the protocol of size-selected, colloidally stable, and biocompatible GO. Further, by using a simple ionic interaction with TMPyP, we prepared a new type of nanotherapeutic agent for an efficient PDT therapy usable in a biologically favorable wavelength. The main aim of this study was to describe the properties and function of a TMPyP photosensitizer in combination with GO by a battery of in vitro tests. Several studies have previously dealt with porphyrins or their derivatives, but only a few reported on using TMPyP in combination with a nanocarrier. We bring a new perspective on the latest in vitro results, including a genotoxicity study of a newly synthesized GO/TMPyP nanocarrier, which makes PDT a suitable candidate for clinical use because of NIR activation and low-light doses.

2. Materials and Methods

The chemicals used in this study included Dulbecco's Modified Eagle Medium (DMEM), phosphate buffered saline (PBS, pH 7.4 own preparation), 5,10,15,20-Tetrakis(1-methyl-4-pyridinio)porphyrin tetra(*p*-toluenesulfonate) (TMPyP Sigma Aldrich, Prague, Czech Republic, 421 nm) 5-(and-6)-chloromethyl-20,70-dichlorodihydrofluorescein diacetate (CM-H_2DCFDA, Invitrogen Co., Waltham, MA, USA), 3-(4,5-dimethyl-2-thiazolyl)-2,5-diphenyl-2H-tetrazolium bromide (MTT, Sigma Aldrich, Prague, Czech Republic), dimethyl sulfoxide (DMSO, Sigma Aldrich Prague, Czech Republic),

HMP agarose (Serva, Biotech), LMP agarose (Qbiogene, Genetica), trypsin, fetal bovine serum (FBS, Sigma Aldrich, Prague, Czech Republic), NaCl (Tamda, Prague, Czech Republic), EDTA (ethylenediaminetetraacetic acid, Lachema), Tris (tris(hydroxymethyl) aminomethane, Sigma Aldrich, Prague, Czech Republic), Triton X-100 (Serva), NaOH (Sigma Aldrich, Prague, Czech Republic) SYBR Green (Invitrogen Co, Waltham, MA, USA), acetone, methanol, and propidium iodide (Sigma Aldrich, Prague, Czech Republic). Graphite powder was obtained from Sigma Aldrich (cat #282863, <20 μm, synthetic) as well as potassium permanganate ($KMnO_4$), sodium nitrate ($NaNO_3$), sulphuric acid (H_2SO_4), and hydrogen peroxide (H_2O_2). Measurements were carried out on multi-detection microplate reader Synergy HT, transmission microscope Olympus IX81 with DSU unit (Olympus, Shinjuku-ku, Japan), and fluorescence/confocal microscope Axio Observer Z1 (Zeiss, Oberkochen, Germany) with a spinning disk CSU X1 (Yokogawa, Musashino, Japan). We used 96-well plates (P-Lab, Prague, Czech Republic) for cell lines cultivation, a glass-bottom Petri dish (Ibidi, Munich, Germany), a glass cover slip (P-lab, Prague, Czech Republic), a centrifugal machine (Biotech, Prague, Czech Republic), and an electrophoretic tank (Bio-RAD, Prague, Czech Republic). Phototox Version 2.0 software (ZEBET, Berlin, Germany) was used for counting IC50 of HeLa cells and Comet Score (TriTek Corp., Sumerduck, VA, USA) for determining the genotoxicity. For cell irradiation, we used LED irradiatiors with 414 nm and 740 nm light-emitting diodes (Kingbright corporation, Taiwan, China, FWHM 20 nm). We used the HeLa cells (human cervical cancer cells) purchased from ATCC (Manassas, VA, USA) and cultivated in low glucose DMEM (Life Technologies, Carlsbad, CA, USA) at 37 °C under 5% CO_2 enriched atmosphere.

2.1. Preparation of Size-Selected Graphene Oxide and Conjugation of Graphene Oxide with TMPyP (GO/TMPyP)

The GO was prepared by a well-established exothermic treatment where graphite powder was oxidized using the Hummers' method. Briefly, concentrated sulfuric acid (23 mL) was added slowly to a mixture of graphite powder (1 g) and sodium nitrate (0.5 g) and cooled to 0 °C. Then, potassium permanganate (3 g) was slowly and in portions added (exothermic process) to this solution and the reaction was maintained below 20 °C. The reaction mixture was then warmed to 35 °C and stirred for an additional 30 min. After being kept at 35 °C for 30 min, distilled water (46 mL) was slowly added (producing another exotherm) and the resulting mixture was stirred at 98° C for 15 min, and cooled to room temperature (RT). Hydrogen peroxide (30%, 1 mL) was then added to the mixture and diluted by 140 mL of distilled water. The resulting material was intensively washed several times with distilled water followed by centrifugation at 6000 rpm for 7 min in order to remove any residual impurities. The obtained material was dried in a vacuum oven overnight to gain graphene oxide powder.

For biomedical applications, it is demanded to have colloidally stable GO particles. Nanometers-sized GO particles were prepared by facile size-sorting of GO powder dispersed in an aqueous solution followed by a simple sonication and centrifugation procedure. At the start, 10 mg of GO powder was dispersed in 20 mL of distilled water with the aid of sonication for 1 h and magnetic stirring overnight, respectively. Subsequently, the centrifugation process at 13,500 rpm for 20 min was followed by decantation of the supernatant solution in order to separate the GO particles of the target size. Then, the conjugation of graphene oxide with TMPyP was performed by mixing positively charged TMPyP with negatively charged GO in water in a molar ratio of 1:1 [22].

2.2. Characterization of GO and GO/TMPyP Was Carried out by Fluorescence Spectroscopy, AFM (Atomic Force Microscopy), and DLS (Dynamic Light Scattering)

Fluorescence spectroscopy was performed on a FLS980 fluorescence spectrometer (Edinburgh Instruments, Livingston, UK) equipped with a R928P photomultiplier (Hamamatsu, Japan) in a thermoelectrically cooled housing, with a 450 W xenon arc lamp as the excitation source for steady-state spectra and an EPL-375 picosecond pulsed diode laser (λ_{em} = 372 nm; Edinburgh Instruments, Livingston, UK) in conjunction with a time-correlated single-photon counting system for time-resolved

fluorescence measurements. The AFM image was obtained in the amplitude-modulated semicontact mode on an NTEGRA Spectra SOLAR (NT-MDT) with upright configuration using an NSG10_DLC AFM probe with the typical tip-curvature radius of 1–3 nm. The amplitude set-point was set to 51% of the cantilever free amplitude; a scanning speed was 0.3 Hz per line, and fresh cleaved muscovite mica was used. The size and Zeta potential (ξ potential) of the selected GO and GO/TMPyP were measured by Zetasizer NanoZS (Malvern, UK). UV/Vis absorption spectra of the GO and GO/TMPyP were obtained by using Specord S600 (Analytic Jena AG, Jena, Germany).

2.3. In Vitro Cell Experiments

2.3.1. Cell and PDT Treatment

HeLa cells (10^4, cervix carcinoma cells) were incubated in a thermobox at 37 °C and 5% CO_2 for 24 h with fresh DMEM. After incubation, DMEM was replaced by a fresh DMEM with sensitizer or a GO/TMPyP nanocarrier. The samples were incubated for 24 h in a thermobox and then washed by PBS. Subsequently, cells in PBS were irradiated by red light using a LED irradiator at a wavelength of 740 nm for 15 min and 33 mW/cm^2 up to the dose of irradiation 30 J/cm^2. Consequently, a violet light LED irradiator was used at a wavelength of 414 nm for 100 s and 10 mW/cm^2 up to the dose of irradiation 1 J/cm^2. After the irradiation, a fresh DMEM was added to the cell culture and the plates were incubated for 0 h (ROS) or 24 h (PS uptake, viability, genotoxicity) in a thermobox at 37 °C and 5% CO_2.

2.3.2. Microscopy Measurement of Cellular Uptake before and after PDT Treatment

In order to use the cell uptake of GO/TMPyP nanocarrier and TMPyP alone, 40,000 cells were cultivated on a glass-bottom Petri dishes with 2 mL DMEM. The cells were fixed in cold methanol/acetone in a ratio of 1:1 for 10 min. The samples were rehydrated in PBS. Microscopic observations were conducted in the confocal microscopy system Axio Observer Z1, equipped with a spinning disk Yokogawa CSU X1, 40 × 0.75 N.A. lens. The measurements were projected for 60 min, 120 min, and 24 h at concentrations of 25 μM. Excitation was performed using 561 nm and 405 nm. Emission was reduced using 404 nm, 465 nm, and 617 nm filters.

2.3.3. MTT Test without and after PDT Treatment

The TMPyP or GO/TMPyP nanocarrier was added at concentrations of 0–25 μM (with respect to TMPyP). The cytotoxic effect and IC50 on the HeLa cells was determined using the MTT assay 24 h after irradiation. We replaced the DMEM with PBS prior to starting the MTT measurements, added 20 μL of 20 mM MTT (dissolved in PBS), and incubated the cells for 3 h at 37 °C and 5% CO_2. The MTT solution was carefully removed and 100 μL of DMSO was added in order to solubilize the violet formazan crystals. The data were calculated by the Phototox Version 2.0 software.

2.3.4. Measurement of Reactive Oxygen Species Kinetic Production

Immediately after the TMPyP and GO/TMPyP nanocarrier irradiation, the ROS kinetic production was assessed for 30 min using CM-H$_2$DCFDA fluorescence probes and microplate reader Synergy HT. The time of the incubation with 5 μM CM-H$_2$DCFDA probes (dissolved in DMSO) was 30 min.

2.3.5. Comet Assay

We adopted the methods from our previous study [23]. Briefly, microscope slides were precoated with 1% HMP agarose. After that, the cells were trypsinized, washed with DMEM with 10% FBS, and centrifuged (6 min, 1000 rpm). An 85 μL of 1% LMP agarose was added to the cell suspension and 85 μL of this mixture was added to the microscope with agarose gel. The microscope slides were immersed in a lysis buffer for 1 h, and then placed in an electrophoretic tank and dipped into a cool electrophoresis solution for 40 min. Electrophoresis was run at 0.8 V/cm and 380 mA for 20 min. Finally,

slides were neutralized in the buffer (0.4 M Tris, pH = 7.5) and the samples were stained with SYBR®
Green and immediately scored using SW Comet Score.

2.3.6. Statistical Analysis

All the data are presented in this article as a mean result ± SD. Statistical differences were evaluated
using the *t*-test and considered significant at $p < 0.05$ level. All figures shown in this article were
obtained from three independent experiments.

3. Results

3.1. Preparation of Size-Selected Graphene Oxide

The GO was prepared by the well-known Hummer's method, but the well-dispersed nanocolloid
of size-selected GO was successfully reached after proper and repeated sonication and centrifugation.
The surface charge of the selected GO, as well as the surface charge of GO/TMPyP nanoconjugate,
was monitored by measuring their ξ potential. The measured ξ potential of the unconjugated GO
corresponded to a charge of –24.6 mV, demonstrating that the free GO has negative charges on its
surface thanks to the hydrophilic oxygen-containing groups [24]. The subsequent conjugation of
TMPyP at the surface of the GO was accompanied by an increase in the material's zeta potential (to
0.6 mV), reflecting the successful conjugation of TMPyP molecules with GO particles. The morphology
of the size-sorted GO was investigated by AFM. Figure 1 shows a freshly sonicated GO deposited by
dropping 2 µL on a mica substrate. Further, it shows height profile along the red line of interest on the
GO particle where the height is about 17 nm and lateral dimensions about 200 nm in length and 79 nm
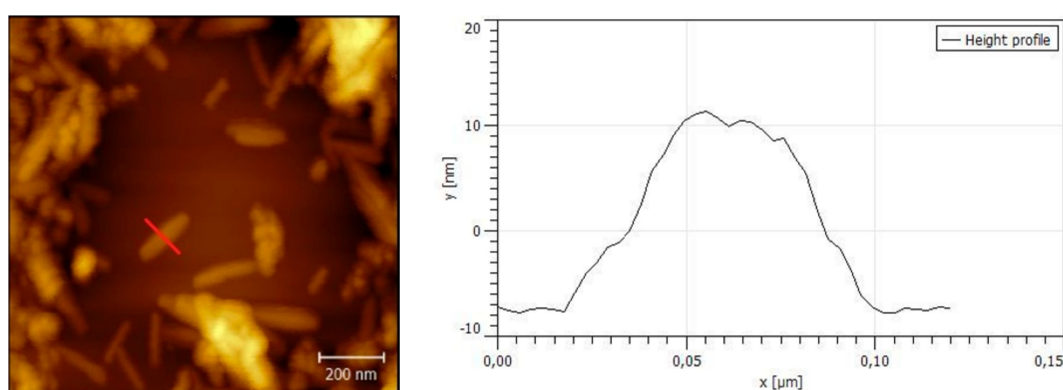in width, this being consistent with the data obtained by the DLS technique (~80 nm).

Figure 1. Atomic force microscopy image of graphene oxide (GO) captured on mica substrate together
with height profile along the red line of interest on GO particle where the height is about 17 nm and
lateral dimension about 200 nm in length.

3.2. Characterization of GO/TMPyP Nanocarrier: (UV–Vis, DLS, Steady-State, and Time-Resolved Fluorescence Spectroscopy)

In order to better understand its formation, the GO/TMPyP nanoconjugate was analyzed by
UV–vis spectroscopy. Due to the negative surface charge of the GO, the TMPyP was easily linked to
the GO in order to form the conjugates of GO/TMPyP by the electrostatic forces, since the TMPyP
is a tetra-cationic porphyrin. In a homogeneous aqueous solution, the TMPyP is characterized by
an absorption maximum of the Soret band at 417 nm (Figure 2, green curve). Optical absorption
spectroscopy was also used to analyze the interaction between the GO and the TMPyP. Figure 2 shows
the absorption spectrum of the GO/TMPyP (black curve) where the strong Soret absorption band at
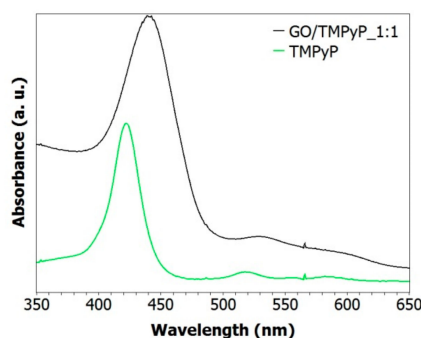417 nm was red-shifted to 437.5 nm, indicating the successful bonding of TMPyP on GO.

Figure 2. UV–vis absorbance spectrum of GO/TMPyP compared to TMPyP and GO alone. There is an obvious red shift of the Soret band from 417 nm (TMPyP) to 4375 nm (GO/TMPyP 1:1).

Figures 3 and 4 show the photoluminescence spectroscopy data for the GO and GO/TMPyP composite. The PL excitation–emission maps of both samples are presented in Figure 3. The emission of TMPyP sample extends from 630 to 800 nm with the excitation wavelength range from 340 to 450 nm. An additional signature in the PL excitation–emission map of the GO/TMPyP composite is visible in the emission range from 400 to 550 nm due to an intrinsic weak emission of the GO. The corresponding emission from the TMPyP in the composite is quenched and its intensity is similar to the one of the GO. The absolute change in the PL intensity can be observed in the PL spectra of the GO and the GO/TMPyP composite under excitation at 370 nm in Figure 4 (left). A broad PL peak of the TMPyP photosensitizer centered at 710 nm (red line) was almost completely quenched in the case of the GO/TMPyP composite (green line) because of an efficient charge transport between the TMPyP and the GO. The latter was also confirmed by PL decay measurements, as depicted in Figure 4 (right). In the case of the GO/TMPyP, the PL lifetime was shortened from 5.3 ns (for neat TMPyP) to 0.7 ns, which was ascribed to an efficient nonradiative charge transfer.
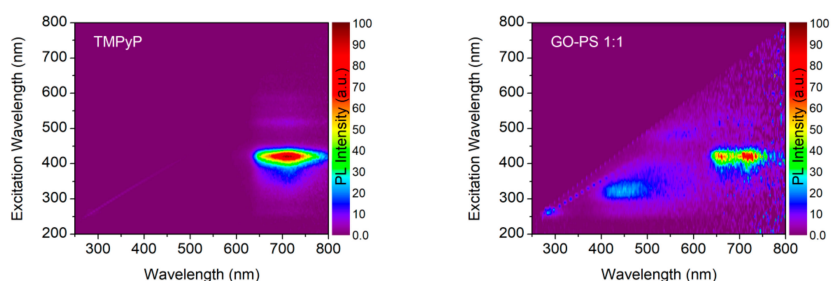

Figure 3. Normalized excitation–emission color maps of TMPyP (**left**) and GO/TMPyP (1:1) (**right**) samples.
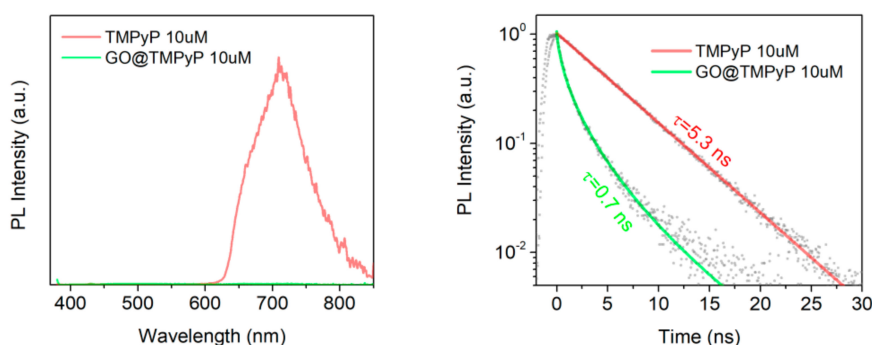

Figure 4. PL emission of TMPyP and GO/TMPyP under the excitation of 375 nm (**left**) and PL decays for TMPyP and GO/TMPyP (**right**). Experimental data are represented by symbols, whereas lines are single or multiexponential fits. Correspondent extracted PL lifetimes are indicated.

3.3. In Vitro Cell Experiments

3.3.1. Microscopy Measurement of Cellular Uptake before and after PDT Treatment

Confocal microscopic analysis showed the distribution of the GO/TMPyP nanocarrier in the HeLa cells (Figure 5). The cell uptake and internalization of the free TMPyP and GO/TMPyP were measured at 60 min, 120 min, and 24 h at 25 μM of TMPyP. TMPyP shows autofluorescence and usually, it emits in two maxima 670 nm and 730 nm [25]. Although the most relevant results are those imaged after 24 h of incubation, which is a usual time for toxicology experiments, it is also substantive to find out the track and distribution of the free TMPyP and GO/TMPyP composite from the beginning of their uptake.

The free TMPyP was distinctly more efficient after 60 min, i.e., the signal was found in the cytoplasm and then in the nucleus more intensely and faster than in the GO/TMPyP nanocarrier (Figure 5A,D). This could be due to the quenching of the TMPyP fluorescence when it is bound on the GO. Nevertheless, after the internalization of the composite, the TMPyP begins to be visible (corresponding to paper [26]). The most probable pathway is endocytosis. The GO/TMPyP composite is gradually subdivided into cytoplasmatic organelles such as lysosomes, where the TMPyP is released and goes directly into the nucleus (Figure 5D,E), as it is seen in 120 min (Figure 5E). By contrast, the free TMPyP is internalized into the nucleus in less than 60 min (Figure 5A). The free TMPyP appears to be completely administrated at the core of the cells after 120 min, and spreads equally. On the other hand, in the GO/TMPyP nanocarrier, the fluorescence signal from the nucleus is different because the nucleosomes are more visible (Figure 5B,E). The rest of the GO/TMPyP nanocarrier or the free GO and free TMPyP is still distributed to cytoplasmic organelles (Figure 5E,F). Finally, the cellular uptake confirmed a targeted delivery of the TMPyP by the GO nanocarrier, followed by the internalization of the TMPyP into the nucleus by the HeLa cells (after 24 h).

In this work, we also studied the morphology of cells and the distribution of agents 24 h after PDT treatment (see Figure 6). It is clearly seen that the cells with the free TMPyP still show adhesion to the surface of the substrate compared to the GO/TMPyP nanocarrier, where the cells are shrunk and, from the morphological view, show apoptotic and necrotic changes. The GO/TMPyP nanocarrier and the free TMPyP are still accumulated in the nucleus of the damaged cells. From these results, we can assume that the GO/TMPyP nanocarrier is more effective in cell damaging.
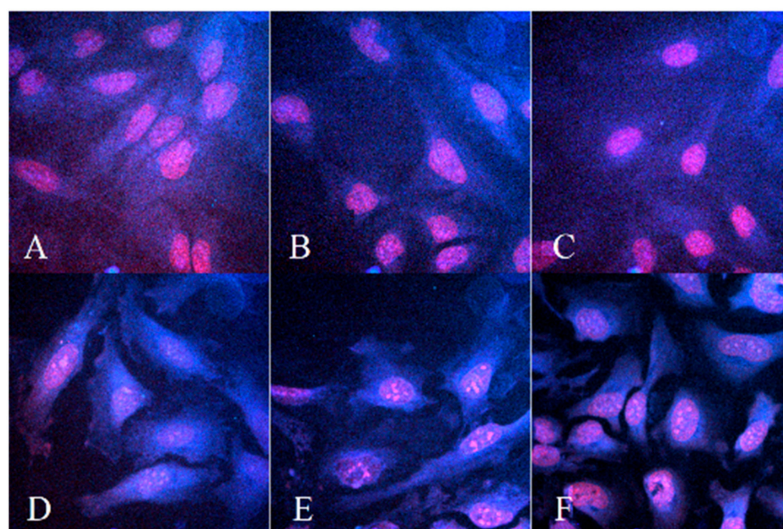

Figure 5. Confocal image of Hela cells after 60 min, 120 min and 24 h of TMPyP (**A**–**C**) and GO/TMPyP nanocarrier (**D**–**F**) at concentration of 25 μM. Red (pink) areas depict TMPyP or GO/TMPyP inside nucleus. Note: (**A**)—60 min TMPyP, (**B**)—120 min TMPyP, (**C**)—24 h TMPyP, (**D**)—60 min GO/TMPyP, (**E**)—120 min GO/TMPyP, (**F**)—24 h GO/TMPyP. Magnification is 40×.
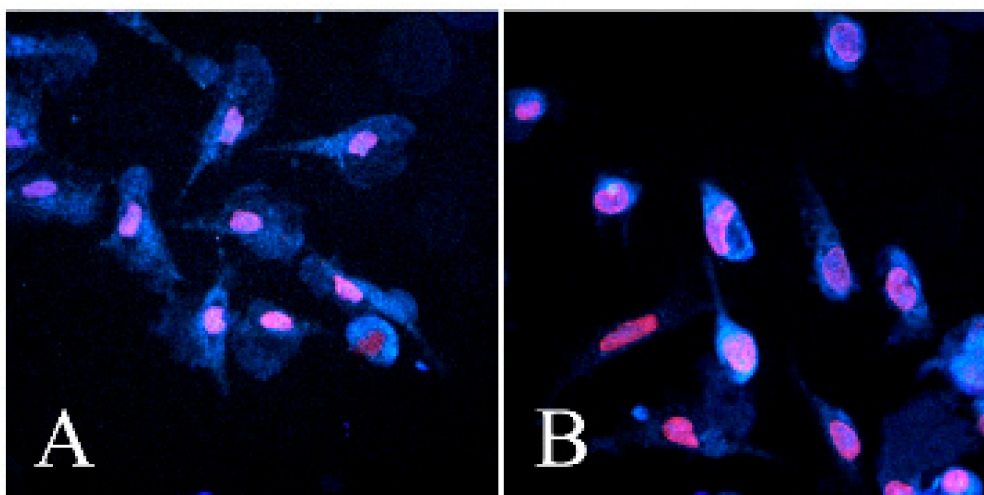
Figure 6. Confocal image 24 h after photodynamic therapy (PDT) treatment (after irradiation with light dose 30 J/cm^2 of 740 nm + light dose 1 J/cm^2 of 414 nm). (**A**)—TMPyP and (**B**)—GO/TMPyP nanocarrier at concentration of 25 μM. Magnification is 40×.

3.3.2. MTT Test without and after Photodynamic Treatments

The effects of the TMPyP and/or GO/TMPyP nanocarriers on the cell viability were determined using MTT assay. The absorbance shows the total metabolic activity of the cell population and is, therefore, an indirect measurement of cell proliferation. Although commonly used as a viability assay, the MTT assay measures the mitochondrial function. The results from the MTT viability assay are presented in the form of IC50 in Table 1.

After 24 h of incubation and PDT irradiation (714 nm and 414 nm), a significant decrease in the cell viability was found in the GO/TMPyP nanocarrier, at concentrations of 3–25 μM. The cell viability decreased with an increasing GO/TMPyP nanocarrier concentration. High level (81–100%) of cell viability was observed in concentrations 0–3 μM. IC50 values show a higher phototoxic effect of the GO/TMPyP nanocarrier (5.275 μM) in comparison with the free TMPyP (8.224 μM). Neither agent, without irradiation, has any effect on the cell viability at the studied concentrations (up to a concentration of 25 μM). Higher concentrations were not studied; however, we suppose a similar effect because these agents show major efficiency after light activation. The GO/TMPyP nanocarrier shows the shift to longer absorption maximum in comparison with the free TMPyP, as you can see in Table 1. By irradiation with 414 nm only, the nanocarrier has no effect on the cell viability (respectively, the viability has not fallen below 50%), but for the free TMPyP, IC50 was set to 8.285 μM.

Table 1. IC50 of TMPyP and GO/TMPyP nanocarrier. Notes: IC50 marked; /, could not be determined due to higher cell viability than 50% at concentrations 0–25 μM.

Treatment	IC50 (μM) TMPyP	IC50 (μM) GO/TMPyP
No irradiation	/	/
740 nm 30 J/cm^2 + 414 nm 1 J/cm^2	8.224	5.2275
414 nm/cm^2 1 J/cm^2	8.285	/

3.3.3. Measurement of Reactive Oxygen Species Kinetic Production

The effect of the free TMPyP and the GO/TMPyP nanocarrier on the ROS formation in the HeLa cells was steadily measured for the first 30 min after the irradiation of 0.25 μM, 2.5 μM, and 25 μM of the TMPyP in both samples. The regression coefficient of the ROS kinetic production determined the rate of the production of the peroxy radical (H_2O_2), hydroxyl radical ($HO^\bullet$), hypochlorous acid

(HOCl), and peroxyl radical (COO$^\bullet$) at each minute of the measurement. The rate of the ROS was calculated using linear regression analysis. A summary of rate values is presented in Figure 7A.
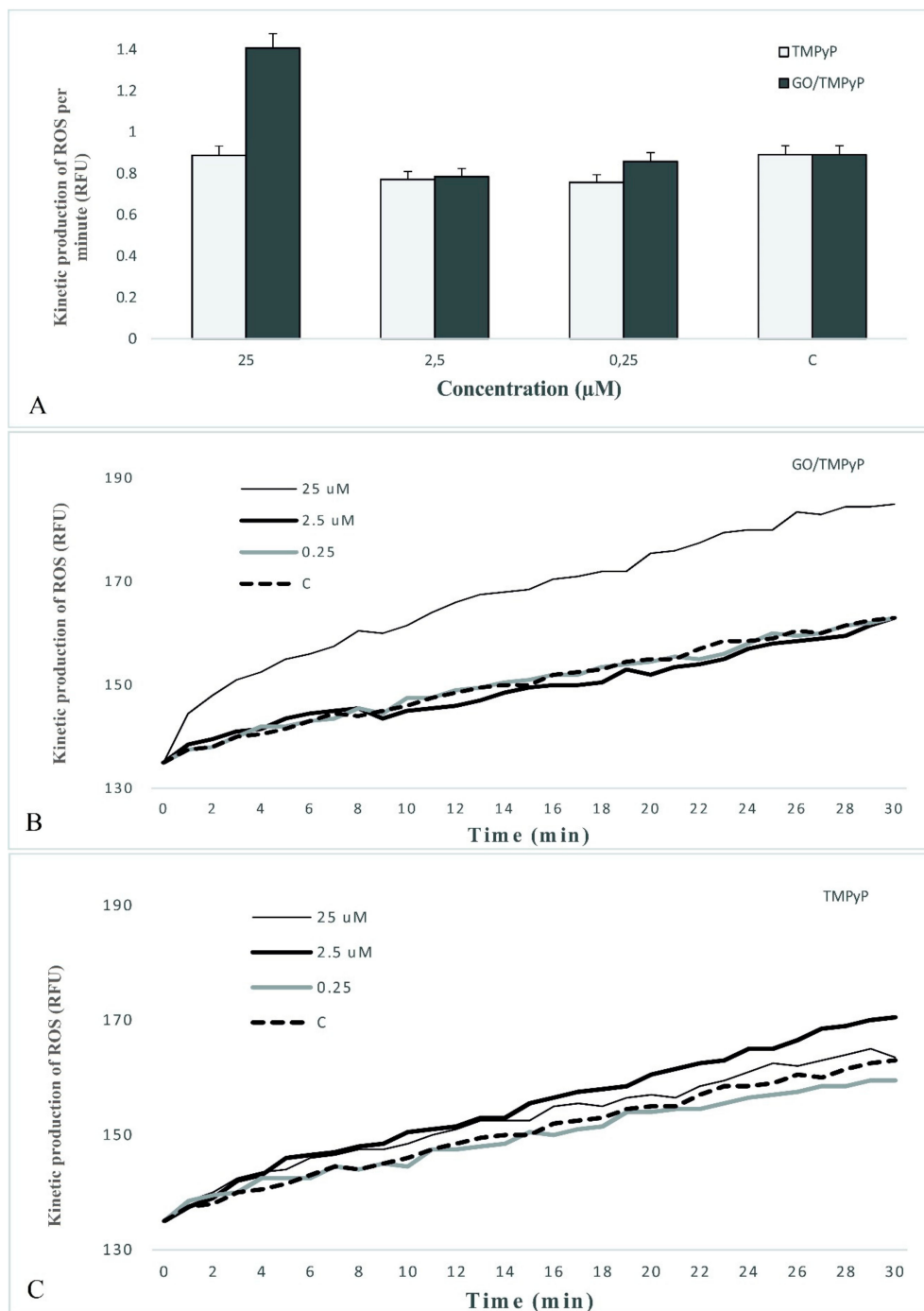

Figure 7. Kinetic production of reactive oxygen species in concentrations of 0.25 μM, 2.5 μM, and 25 μM of TMPyP (**A,C**) or GO/TMPyP (**A,B**) nanocarrier on the HeLa cell line. Notes: The linear regression of the reactive oxygen species (ROS) rate expressed the ROS amount created at each minute. Data represent mean and standard error from three independent measurements.

The data present an enhancement in the generation of ROS between the control and the GO/TMPyP nanocarrier at a concentration of 25 μM. The comparison of the free TMPyP and the GO/TMPyP nanocarrier at a 25 μM concentration shows a considerably higher reactive oxygen species generation in

the GO/TMPyP nanocarrier within the first 30 min after the irradiation (Figure 7B and 7C). These results show the feasible increase of the cytotoxic influence of the GO/TMPyP nanocarrier when incorporated into the HeLa cells via the ROS pathway.

3.3.4. Comet Assay

Comet assay is an analysis for genotoxicity assessment. We determined the fragmentation of DNA after 24 h of the PDT. The tail length and the percentage of DNA in tail are depicted as histograms in Figure 8. Tail length and % of DNA in tail were significantly greater at all tested concentrations (0.25 μM, 2.5 μM, and 25 μM) in both agents, the free TMPyP and the GO/TMPyP nanocarrier in comparison to the control groups. As we can see in graphs, the GO/TMPyP nanocarrier has significantly higher genotoxic potential at all concentrations compared with the free TMPyP. Only at a concentration of 25 μM in the free TMPyP, the higher % of DNA in tail was observed in comparison with the GO/TMPyP nanocarrier (Figure 8A). However, in the same concentration, total tail length and comet length was higher, and we marked it as a higher impact (Figure 8B).
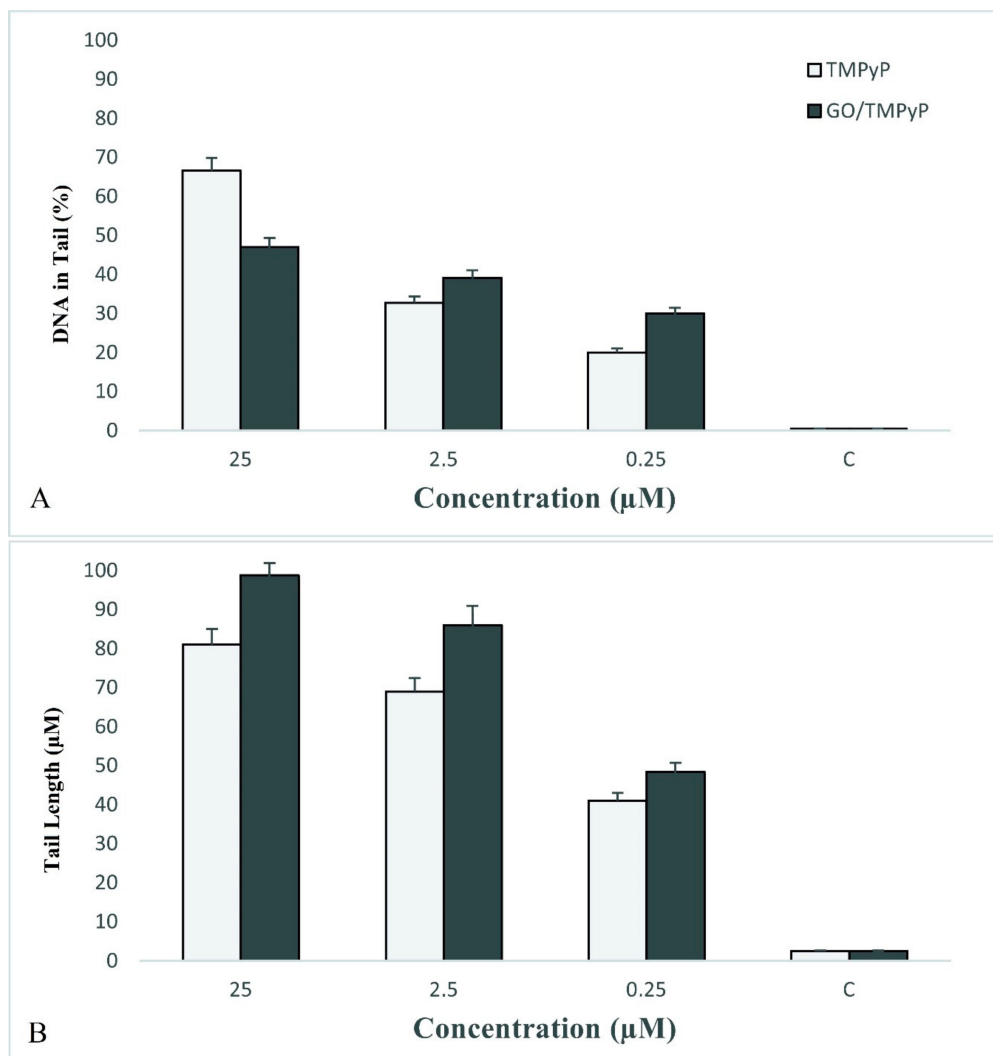
Figure 8. Percentage of DNA in tail (**A**) and tail length (**B**) determined by comet assay in concentrations of 25 μM, 2.5 μM, and 0.25 μM of TMPyP and GO/TMPyP nanocarrier on the HeLa cell lines. Data represent mean and standard error from three independent measurements.

4. Discussion

Recently, based on the advantages of nanoparticles, using biocompatible nanoparticles as vehicles to deliver a targeting ligand for targeted cancer treatment and targeted imaging has drawn increasing attention [27–31]. This innovative approach increases the accumulation of the nanoparticle delivery carriers in tumor sites and induces enhanced therapeutic, permeability, and retention effects.

Here, we developed and verified the protocol for the synthesis of biocompatible graphene oxide with defined size and charge (~80 nm measured by DLS and −24.6 mV from zeta potential measurements). Optimizing the post-synthetic procedure such as a facile size-sorting of GO powder dispersed in an aqueous solution by a simple sonication and subsequent centrifugation procedure (see Figure 1) caused that the as-prepared GO nanoparticles are colloidally stable with the size appropriate for biomedical applications, along with revealing extraordinary biocompatibility [32].

Successful conjugation of TMPyP molecules on the GO sheet is clearly demonstrated in Figure 2, where the UV–vis spectrum indicates an obvious red shift of the Soret band from 417 to 437.5 nm. Similar results have been described by [33]. This spectral shift is due to the molecular flattening of TMPyP after the assembly with GO. Firstly, the electrostatic interaction of TMPyP and GO was observed, as it is confirmed by changing the resulting zeta potential. Then π–π stacking interactions induced the flattening of TMPyP molecules and enlarged the π conjugation of the porphyrin system. Moreover, the effective nonradiative charge transfer between GO conjugated on TMPyP has been observed where a PL peak of a TMPyP photosensitizer was almost completely quenched (Figures 3 and 4, left). This phenomenon was confirmed also by the PL decay measurements where the PL lifetime of TMPyP was shortened from 5.3 ns to 0.7 ns for GO/TMPyP nanocarrier (Figure 4, right).

The main aim of this study was the comparison of the photosensitivity and in vitro cytotoxic effect of cationic photosensitizer TMPyP and GO/TMPyP nanocarrier to cancer cell line HeLa. Cationic porphyrins are known as effective photodynamic sensitizers which can selectively photocleave DNA and inhibit telomerases [34]. There is a given rule prescribed by ANSI (American National Standards Institute) that maximum permissible exposure of skin for 808 and 980 nm wavelengths is 330–350 mW/cm^2 with an exposure time of 10–1000 s. Therefore, it is highly desirable to develop an effective and biocompatible light-activatable reagent, which can operate under low-light doses. In our study, we developed a nanocarrier for targeted delivery of TMPyP and irradiated HeLa cells by using 740 nm wavelength with 33 mW/cm^2 with exposure time 900 s and 414 nm wavelength with 10 mW/cm^2 with exposure time 100 s.

The new type of a GO/TMPyP nanocarrier provides very favorable conditions for clinical use, also because of shifting to longer wavelengths which will provide enhanced tissue penetration. Viability results of cells not being treated by PDT show good biocompatibility of the nanocarrier; however, after irradiation at a wavelength of 740 nm and 414 nm, cell destruction and loss of cell viability were observed more significantly than in the free TMPyP. We suggested that thanks to the known photothermal effect of graphene, the TMPyP could be more easily delivered by means of local heating using 740 nm laser, as already observed for different photosensitizers in [26].

The uptake of a photosensitizer by a cancer cell is a critical factor that affects the treatment efficacy or cancer cell imaging. Here, the cellular uptake of TMPyP on HeLa cells was studied using confocal fluorescence microscopy. During the first stage (up to 60 min after addition of PSs), the TMPyP or GO/TMPyP nanocarrier was only localized with different density in cytoplasmatic organelles (lysosomes and mitochondria). The same result achieved Zhu et al. [35]. They studied the localization of H_2TMPyP in the endoplasmic reticulum, Golgi apparatus, lysosomal, and mitochondria in HK-1 cells. The lysosomal membrane protein is mostly glycoprotein. Besides, the lysosomal membrane also contains a special transport protein that uses the energy of ATP hydrolysis to pump cytoplasmic H^+ into the lysosome in order to maintain its pH 5. Thus, the weak acid biological environment could make the amidinophenylporphyrins gather in the lysosomal of the cells [35]. After 120 min, PS is loaded to the nucleus. Due to the administration of PS to the nucleus, after irradiation with appropriate wavelength, DNA damage occurs.

ROS, the major mechanism of action of free TMPyP, is described as TMPyP-induced production of ROS. Pizova et al. observed extensive changes after ROS cell oxidation on a cellular and molecular level (ROS production, cell death induction, changes in *C-FOS*, and *C-MYC* expression) after TMPyP light activation (413 nm, 5 J/cm^2) on MCF7 and G361 cancer cell lines [11]. On the other hand, TMPyP loaded on hp-β-cyclodextrin shows a higher effect on non-cancer cell NIH3T3 than cancer cell line HeLa [36]. ROS located in mitochondria can be detected probably due to producing superoxide radicals after the uptake of PS. The main purpose of PS is to produce ROS via the reduction of electrons to free radicals, which then react with oxygen [37]. Here, we observed the increase in the ROS production level of GO/TMPyP compared to TMPyP at a concentration of 25 μM, indicating the higher cellular uptake and /or higher electron (charge) transfer and therefore higher PDT efficacy. This fact was nicely visible in images from confocal microscopy, where after the PDT treatment the cells with GO/TMPyP were deadhered and changed drastically their native morphology, compared to TMPyP treated cells only. The oxidative stress of the TMPyP and GO/TMPyP on the cells may cause DNA damage, changes in cell cycle progression, and genotoxicity.

Genotoxicity of the TMPyP and GO/TMPyP nanocarrier was determined by comet assay. The uptake of PS to the nucleus leads to DNA damage after irradiation. As Csík et al. referred, photoinduced reaction of bound TMPyP caused alterations in DNA structures and DNA–protein interactions within both nucleoprotein complexes; the nucleosomes were found to be more sensitive to the photoreaction [38]. Other work observed cell photocytotoxicity research of TPMPyP$_2$ and TMPyP$_2$, with a better antitumor effect of TPMPyP$_2$ thanks to higher G-quadruplexes DNA binding affinity [39].

In a similar study on a GO nanocarrier, a GO/Ce6 nanocomposite was prepared and tested for its PDT efficacy on KB cancer cells [26]. However, compared to our system, they used 10 times higher power of light to observe effective cell killing. For the next step, we continue to prepare our system for selective and in vivo applications.

5. Conclusions

To sum up, we present a first in vitro study on a GO/TMPyP composite for PDT in clinically approved standards for light activation and in biologically favorable wavelengths.

We have shown that in vitro effects of new a GO/TMPyP nanocarrier differed in comparison with a free TMPyP. The cellular uptake confirmed possible targeted delivery of the GO/TMPyP nanocarrier followed by internalization of the TMPyP in the nuclei of HeLa cells. Contrary to the free TMPyP after irradiation with biologically favorable wavelengths, the GO/TMPyP nanocarrier showed higher ROS values and higher DNA damage followed by induction of apoptosis. This fact makes a GO/TMPyP a potential candidate for clinical use in the future.

References

1.　WHO Cancer Facts. Available online: https://www.who.int/news-room/fact-sheets/detail/cancer (accessed on 12 September 2018).

2.　Jemal, A.; Siegel, R.; Ward, E.; Hao, Y.; Xu, J.; Thun, M.J. Cancer Statistics 2009. *CA Cancer J. Clin.* **2009**, *59*, 225–249. [CrossRef] [PubMed]

3. Jemal, A.; Center, M.M.; DeSantis, C.; Ward, E.M. Global patterns of cancer incidence and mortality rates and trends. *Cancer Epidemiol. Biomark. Prev.* **2010**, *19*, 1893–1907. [CrossRef] [PubMed]

4. Dolmans, D.E.; Fukumura, D.; Jain, R.K. Photodynamic therapy for cancer. *Nat. Rev. Cancer* **2003**, *3*, 380–387. [CrossRef] [PubMed]

5. Huang, Z.; Xu, H.; Meyers, A.D.; Musani, A.I.; Wang, L.; Tagg, R. Photodynamic therapy for treatment of solid tumors—Potential and technical challenges. *Technol. Cancer Res. Treat.* **2008**, *7*, 309–320. [CrossRef] [PubMed]

6. Wilson, B.C.; Patterson, M.S. The physics, biophysics and technology of photodynamic therapy. *Phys. Med. Biol.* **2008**, *53*, 61–109. [CrossRef]

7. Malina, L.; Tomankova, K.B.; Malohlava, J.; Jiravova, J.; Manisova, B.; Zapletalova, J.; Kolarova, H. The in vitro cytotoxicity of metal-complexes of porphyrin sensitizer intended for photodynamic therapy. *Toxicol. Vitro* **2016**, *34*, 246–256. [CrossRef] [PubMed]

8. Robertson, C.A.; Evans, D.; Abrahamse, H. Photodynamic therapy (PDT): A short review on cellular mechanisms and cancer research applications for PDT. *J. Photochem. Photobiol. B Biol.* **2009**, *96*, 1–8. [CrossRef]

9. Castano, A.P.; Mroz, P.; Hamblin, M.R. Photodynamic therapy and anti-tumor immunity. *Nat. Rev. Cancer* **2006**, *6*, 535–545. [CrossRef]

10. Tapajos, E.C.C.; Longo, J.P.; Simioni, A.R.; Lacava, Z.G.M.; Santos, M.F.M.A.; Morais, P.C.; Tedesco, A.C.; Azevedo, R.B. In vitro photodynamic therapy on human oral keratinocytes using chloroaluminum-phthalocyanine. *Oral Onkol.* **2008**, *44*, 1073–1079. [CrossRef]

11. Pizova, K.; Bajgar, R.; Fillerova, R.; Kriegova, E.; Cenklova, V.; Langova, K.; Konecny, P.; Kolarova, H. C-*MYC* and C-*FOS* expression changes and cellular aspects of the photodynamic reaction with photosensitizers TMPyP and ClAlPcS$_2$. *J. Photochem. Photobiol. B Biol.* **2015**, *142*, 186–196. [CrossRef]

12. Tomankova, K.; Polakova, K.; Pizova, K.; Binder, S.; Havrdova, M.; Kolarova, M.; Kriegova, E.; Zapletalova, J.; Malina, L.; Malohlava, J.; et al. In vitro cytotoxicity analysis of doxorubicin loaded/superparamagnetic iron oxide colloidal nanoassemblies on MCF7 and NIH3T3 cell lines. *Int. J. Nanomed.* **2015**, *10*, 949–961. [CrossRef] [PubMed]

13. Koo, O.M.; Rubinstein, I.; Onyuksel, H. Role of nanotechnology in targeted drug delivery and imaging: A concise review. *Nanomed. NBM* **2005**, *3*, 193–212. [CrossRef] [PubMed]

14. Chen, H.; Zhang, W.; Zhu, G.; Xie, J.; Chen, X. Rethinking cancer nanotheranostics. *Nat. Rev. Mater.* **2017**, *2*, 1–18. [CrossRef]

15. Min, Y.; Caster, J.M.; Eblan, M.J.; Wang, A.Z. Clinical translation of nanomedicine. *Chem. Rev.* **2015**, *115*, 11147–11190. [CrossRef] [PubMed]

16. Shi, J.; Kantoff, P.W.; Wooster, R.; Farokhzad, O.C. Cancer nanomedicine: Progress, challenges and opportunities. *Nat. Rev. Cancer* **2017**, *17*, 20–37. [CrossRef] [PubMed]

17. Allen, M.J.; Tung, V.C.; Kaner, R.B. Honeycomb Carbon: A Review of Graphene. *Chem. Rev.* **2010**, *110*, 132–145. [CrossRef]

18. Tucek, J.; Sofer, Z.; Bousa, D.; Pumera, M.; Hola, K.; Mala, A.; Polakova, K.; Havrdova, M.; Cepe, K.; Tomanec, O.; et al. Air-stable superparamagnetic metal nanoparticles entrapped in graphene oxide matrix. *Nat. Commun.* **2016**, *7*, 12879. [CrossRef]

19. Xu, Z.; Wang, S.; Li, Y.; Wang, M.; Shi, P.; Huang, X. Covalent functionalization of graphene oxide with biocompatible poly(ethylene glycol) for delivery of paclitaxel. *ACS Appl. Mater. Interfaces* **2014**, *6*, 17268–17276. [CrossRef] [PubMed]

20. Zhang, L.; Yang, X.; Zhang, F.; Long, G.; Zhang, T.; Leng, K.; Zhang, Y.; Huang, Y.; Ma, Y.; Zhang, M.; et al. Controlling the Effective Surface Area and Pore Size Distribution of sp2 Carbon Materials and Their Impact on the Capacitance Performance of These Materials. *J. Am. Chem. Soc.* **2013**, *135*, 5921–5929. [CrossRef]

21. Xu, Y.; Zhao, L.; Bai, H.; Hong, W.; Li, C.; Shi, G. Chemically Converted Graphene Induced Molecular Flattening of 5,10,15,20- tetrakis(1-methyl-4-pyridinio)porphyrin and Its Application for Optical Detection of Cadmium(II) Ions. *J. Am. Chem. Soc.* **2009**, *131*, 13490–13497. [CrossRef]

22. Özçakır, E.; Eskizeybek, V. A facile and effective method for size sorting of large flake graphene oxide. In Proceedings of the World Congress on Recent Advances in Nanotechnology (RAN'16), Prague, Czech Republic, 1–2 April 2016. [CrossRef]

23. Tomankova, K.; Kejlova, K.; Binder, S.; Daskova, A.; Zapletalova, J.; Bendova, H.; Kolarova, H.; Jirova, D. In vitro cytotoxicity and phototoxicity study of cosmetics colorants. *Toxicol. Vitro* **2011**, *25*, 1242–1250. [CrossRef]

24. Wychowaniec, J.K.; Iliut, M.; Zhou, M.; Moffat, J.; Elsawy, M.A.; Pinheiro, W.A.; Hoyland, J.A.; Miller, A.F.; Vijayaraghavan, A.; Saiani, A. Designing Peptide/Graphene Hybrid Hydrogels through Fine-Tuning of Molecular Interactions. *Biomacromolecules* **2018**, *19*, 2731–2741. [CrossRef] [PubMed]

25. Bornhütter, T.; Pohl, J.; Fischer, C.; Saltsman, I.; Mahammed, A.; Gross, Z.; Röder, B. Development of Singlet Oxygen Luminescence Kinetics during the Photodynamic Inactivation of Green Algae. *Molecules* **2016**, *21*, 485. [CrossRef] [PubMed]

26. Tian, B.; Wang, C.; Zhang, S.; Feng, L.; Liu, Z. Photothermally Enhanced Photodynamic Therapy Delivered by Nano-Graphene Oxide. *ASC Nano* **2011**, *5*, 7000–7009. [CrossRef]

27. Mixhalet, X.; Pinaud, F.F.; Bentolila, L.A.; Tsay, J.M.; Doose, S.; Li, J.J.; Sundaresan, G.; Wu, A.M.; Gambhir, S.S.; Weiss, S. Quantum Dots for Live Cells, in Vivo Imaging, and Diagnostics. *Science* **2005**, *307*, 538–544. [CrossRef] [PubMed]

28. Yu, X.; Trase, I.; Ren, M.; Duval, K.; Guo, X.; Chen, Z. Design of Nnaoparticle-Based carrieres for targeted drug delivery. *J. Nanomater.* **2016**, *2016*, 1087250. [CrossRef] [PubMed]

29. Yong, K.T.; Roy, I.; Swihart, M.T.; Prasad, P.N. Multifunctional nanoparticles as biocompatible targeted probes for human cancer diagnosis and therapy. *J. Mater. Chem.* **2009**, *19*, 4655–4672. [CrossRef] [PubMed]

30. Azzazy, H.M.E.; Mansour, M.M.H.; Kazmierczak, S.C. From diagnostics to therapy: Prospects of quantum dots. *Clin. Biochem.* **2007**, *40*, 917–927. [CrossRef]

31. Prasad, P.N. *Nanophotonics*; Wiley-Interscience: New York, NY, USA, 2004.

32. Marcano, D.C.; Kosynkin, D.V.; Berlin, J.M.; Sinitskii, A.; Sun, Z.; Slesarev, A.; Alemany, L.B.; Lu, W.; Tour, J.M. Improved synthesis of graphene oxide. *ACS Nano* **2010**, *4*, 4806–4814. [CrossRef]

33. Xu, X.L.; Lin, F.W.; Du, Y.; Zhang, X.; Wu, J.; Xu, Z.K. Graphene Oxide Nanofiltration Membranes Stabilized by Cationic Porphyrin for High Salt Rejection. *ACS Appl. Mater. Interfaces* **2016**, *8*, 12588–12593. [CrossRef]

34. Mosinger, J.; Slavětínská, L.; Lang, K.; Coufal, K.; Kubát, P. Cyclodextrin carriers of positivelycharged porphyrin sensitizers. *Org. Biomol. Chem.* **2009**, *7*, 3797–3804. [CrossRef] [PubMed]

35. Zhu, S.; Wu, F.; Wang, K.; Zheng, Y.; Li, Z.; Zhang, X.; Wong, W.K. Photocytotoxicity, cellular uptake and subcellular localization of amidinophenylporphyrins as potential photodynamic therapeutic agents: An in vitro cell study. *Bioorg. Med. Chem. Lett.* **2015**, *25*, 4513–4517. [CrossRef] [PubMed]

36. Hanakova, A.; Bogdanova, K.; Tomankova, K.; Pizova, K.; Malohlava, J.; Binder, S.; Bajgar, R.; Langova, K.; Kolar, M.; Mosinger, J.; et al. The application of antimicrobial photodynamic therapy on S. aureus and E. coli using porphyrin photosensitizers bound to cyclodextrin. *Microbiol. Res.* **2014**, *169*, 163–170. [CrossRef] [PubMed]

37. Lüpertz, R.; Wätjen, W.; Kahl, R.; Chovolou, Y. Dose- and time-dependent effects of doxorubicin on cytotoxicity, cell cycle and apoptotic cell death in human colon cancer cells. *Toxicology* **2010**, *271*, 115–121. [CrossRef]

38. Csík, G.; Egyeki, M.; Herényi, L.; Majer, Z.; Tóth, K. Role of structure-proteins in the porphyrin–DNA interaction. *J. Photochem. Photobiol. B Biol.* **2009**, *96*, 207–215. [CrossRef]

39. Zhao, P.; Liu, M.-C.; Zheng, M.; Jin, S.F.; Tang, D.T.; Chen, J.; Ma, Y.-A.; Lin, J.-Q.; Wang, X.-H.; Liu, H.J. G-quadruplex DNA interactions, docking and cell photocytotoxicity research of porphyrin dyes. *Dyes Pigment.* **2016**, *128*, 41–48. [CrossRef]